

Reconfigurable Intelligent Surface for mmWave Mobile Communications: What If LoS Path Exists?

Baiping Xiong[✉], Zaichen Zhang[✉], Senior Member, IEEE, and Hao Jiang[✉], Member, IEEE

Abstract—Reconfigurable intelligent surface (RIS) has been widely discussed owing to its potential in enhancing the communication performance in a low-cost and energy efficient manner. The existing research on RIS-assisted channel modeling is mainly based on the assumption of obstructed line-of-sight (LoS) path between the transceivers. However, what if the LoS path (re)appears in RIS-assisted mobile communications? This letter aims at answering this question by developing a novel non-stationary channel model for RIS auxiliary millimeter wave (mmWave) mobile systems in the presence of alternately disappearing and reappearing LoS path. Based on the proposed channel model, a transmission mode switch scheme at a base station (BS) is developed based on the time-varying location of the receiver. The mapping relationship between BS transmission mode and receiver location is derived. Numerical results are provided to verify our analysis.

Index Terms—Reconfigurable intelligent surface, (re)appearing LoS path, mmWave channel model, transmission mode switch.

I. INTRODUCTION

Millimeter wave (mmWave) communications are witnessed to be a potential solution to meet with the increasing data rate and spectrum resources demands of future wireless networks [1]. Owing to the high path loss, mmWave communications heavily rely on directional transmission through line-of-sight (LoS) link with beamforming, whose performance can be easily and severely deteriorated when the LoS path gets blocked. The recently emerging reconfigurable intelligent surface (RIS) technology is considered promising to address this issue in a cost/energy/spectral efficient manner by contributing a virtual LoS (V-LoS) link between the transceiver [2].

Manuscript received 31 October 2022; accepted 11 November 2022. Date of publication 15 November 2022; date of current version 10 February 2023. This work was supported in part by the National Key Research and Development Program of China under Grant 2020YFB1806603; in part by NSFC Projects under Grant 62101275, Grant 61960206005, Grant 62101127, Grant 61971136, Grant 62171127, and Grant 61803211; in part by the Fundamental Research Funds for the Central Universities under Grant 2242022k30001; in part by the Jiangsu NSF Projects under Grant BK20200393 and Grant BK20200820; and in part by the Research Fund of National Mobile Communications Research Laboratory. The associate editor coordinating the review of this article and approving it for publication was I. Al-Nahhal. (*Corresponding author: Zaichen Zhang*)

Baiping Xiong and Zaichen Zhang are with the National Mobile Communications Research Laboratory, Frontiers Science Center for Mobile Information Communication and Security, Southeast University, Nanjing 210096, China, and also with the Pervasive Communication Research Center, Purple Mountain Laboratories, Nanjing 211111, China (e-mail: xiongbp@seu.edu.cn; czhang@seu.edu.cn).

Hao Jiang is with the College of Artificial Intelligence, Nanjing University of Information Science and Technology, Nanjing 210044, China, and also with the National Mobile Communications Research Laboratory, Southeast University, Nanjing 210096, China (e-mail: jianghao@nust.edu.cn).

Digital Object Identifier 10.1109/LWC.2022.3222164

In the literature, RIS-assisted wireless communications have been studied for data rate improvement and coverage enhancement. Specifically, the authors in [3] demonstrated that the channel capacity of an indoor mmWave system is significantly improved after the deployment of RIS. In [4], the outage and average bit-error probabilities of a RIS-assisted mmWave system is investigated and shown to outperform that of amplify-and-forward (AF) relay system. The authors in [5] studied the blindness compensation for RIS-assisted mmWave communications by jointly optimizing the transmit precoding vector, RIS reflection phase matrix, and RIS's location.

In general, the existing work has mainly assumed a blocking LoS link in RIS-assisted channel modeling. Several works such as [6] have considered direct link, but are restricted for stationary systems. In future mobile wireless networks, the communication environment is changeable due to the high dynamic properties of the transmitter/receiver/clusters. This indicates that the LoS link is not always blocked or existing, and will experience alternately disappearing and reappearing. In this case, the existing results may not hold, and therefore motivates us to reconsider the channel modeling and transmission strategy design of RIS-assisted mobile communications with (re)appearing LoS path. In this letter, we propose a novel non-stationary channel model for RIS-assisted mmWave mobile systems with (re)appearing LoS path. Then, a base station (BS) transmission mode switch scheme is developed in the offline stage, which motivates BS to switch its transmission mode by adopting different beamforming vectors when mobile receiver (MR) moves into different sub-areas in the online stage. We derive the mapping relationship between BS transmission mode and MR location, and analyze how the system setup influence the mapping relationship.

Notation: Throughout this letter, non-boldface, boldface lowercase, and boldface uppercase letters denote scalar, vector, and matrix, respectively; $|\cdot|$, $(\cdot)^T$, $(\cdot)^*$, and $\langle \cdot \rangle$ stand for absolute value, transpose, complex conjugate, and vector dot product, respectively; $\mathbb{E}(\cdot)$, \cap , \cup , and \ominus take the expectation, intersection set, union set, and difference set, respectively.

II. SYSTEM MODEL

As shown in Fig. 1, let us consider a RIS auxiliary three-dimensional (3D) multiple-input multiple-output (MIMO) mmWave mobile communication scenario with one static BS, one moving MR with speed v_R and direction γ_R , and one pre-deployed static RIS. The small wavelength of mmWave enables more RIS units to be fabricated without increasing array dimension. The BS and MR are both equipped with omnidirectional uniform linear arrays (ULAs) with antenna numbers M_T and M_R , respectively, as well as antenna element spacings δ_T and δ_R , respectively. The RIS,

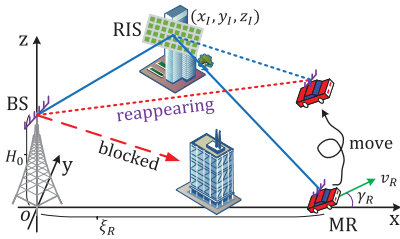


Fig. 1. A physical illustration of the proposed RIS auxiliary mmWave mobile communications with reappearing LoS path.

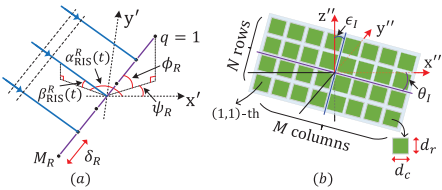


Fig. 2. Angles definitions: (a) definition of AoA (AAoA and EAoA) angle and MR's ULA orientation angles; (b) definition of RIS orientation angles. The axes in the x' - y' and x'' - y'' - z'' are parallel to those in x - y - z of Fig. 1.

TABLE I
SUMMARY OF KEY PARAMETERS DEFINITIONS

$\xi_{\text{TR}}(t)$	distance between BS and MR
$\alpha_T^{\text{LoS}}(t), \beta_T^{\text{LoS}}(t)$	AAoD and EAoD of LoS link
$\alpha_R^{\text{LoS}}(t), \beta_R^{\text{LoS}}(t)$	AAoA and EAoA of LoS link
$\xi_{\text{RIS}}, \xi_{\text{RIS}}^R(t)$	distances between BS/MR and RIS
$\xi_{mn}, \xi_{mn}^R(t)$	distances between BS/MR and (m, n) -th RIS unit
$\alpha_{\text{RIS}}^T, \beta_{\text{RIS}}^T$	AAoD and EAoD from BS to RIS
$\alpha_{\text{RIS}}^R(t), \beta_{\text{RIS}}^R(t)$	AAoA and EAoA from RIS to MR
α_i, β_i	azimuth/normal incident angles on RIS from BS
$\alpha_o(t), \beta_o(t)$	azimuth/normal reflected angles from RIS to MR

which is a uniform planar array (UPA), has $M \times N$ reflecting units consisting of M columns and N rows. The size of each RIS unit is denoted by $d_c \times d_r$. At the initial instant, i.e., $t = 0$, the locations of the central points of BS's ULA, RIS, and MR's ULA are denoted by $(0, 0, H_0)$, (x_I, y_I, z_I) , and $(\xi_R, 0, 0)$, respectively. In this letter, we consider a more practical antenna setup by introducing ψ_T and ϕ_T to describe the azimuth and elevation orientation angles of BS's ULA, and at the MR side they are denoted by ψ_R and ϕ_R [7], as depicted in Fig. 2(a). Moreover, instead of deploying the RIS on the x'' - z'' plane, we assume that the RIS is deployed with a rotation angle of ϵ_I about z'' -axis and a rotation angle of θ_I about x'' -axis, respectively, as shown in Fig. 2(b). This enhances the scope of the proposed model to describe the realistic RIS-assisted communication scenarios. Other parameters are summarized in Table I.

For clarity, we assume that the BS communicates one data stream with MR, the extension to multiple data streams scenario is straightforward and will not affect the final results. We define s as the transmitted symbol with power $\mathbb{E}\{ss^*\} = P_T$, $\mathbf{H}_{\text{TR}}(t, f) \in \mathbb{C}^{M_R \times M_T}$ as the frequency domain channel matrix, and then the corresponding complex baseband received signal model can be expressed as [8], [9]

$$y(t) = \mathbf{f}_{\text{MR}}^T(t) \mathbf{H}_{\text{TR}}(t, f) \mathbf{f}_{\text{BS}}(t) s + n(t), \quad (1)$$

where $n(t)$ is the noise component and is assumed to be a zero-mean complex Gaussian process with variance σ^2 , and

$\mathbf{f}_{\text{BS}}(t) \in \mathbb{C}^{M_T \times 1}$ and $\mathbf{f}_{\text{MR}}(t) \in \mathbb{C}^{M_R \times 1}$ denote the BS transmit beamforming and MR receive combining vectors, respectively. As the MR moves, the LoS link will reappear and disappear alternately, making the channel $\mathbf{H}_{\text{TR}}(t, f)$ changeable and hence arising for the requirement of reconsideration of BS transmit beamforming vector $\mathbf{f}_{\text{BS}}(t)$ design.

We firstly introduce the channel model applicable for RIS auxiliary mmWave mobile communications with (re)appearing LoS path. Benefit from the directional transmission by beamforming, we ignore the non-LoS components due to their negligible power gains. Then, the complex time domain channel characteristics between BS and MR can be described by $\mathbf{H}_{\text{TR}}(t, \tau) = \int \mathbf{H}_{\text{TR}}(t, f) e^{j2\pi f\tau} df = [h_{pq}(t, \tau)]_{M_R \times M_T}$, where $h_{pq}(t, \tau)$ denotes the complex channel impulse response (CIR) including large-scale path loss between the p -th ($p = 1, 2, \dots, M_T$) BS antenna and the q -th ($q = 1, 2, \dots, M_R$) MR antenna and can be expressed as [10]

$$h_{pq}(t, \tau) = \sqrt{\Omega_{\text{LoS}}(t)} \cdot h_{pq}^{\text{LoS}}(t) \delta(\tau - \tau^{\text{LoS}}(t)) + \sqrt{\Omega_{\text{RIS}}(t)} \cdot h_{pq}^{\text{V-LoS}}(t) \delta(\tau - \tau^{\text{V-LoS}}(t)), \quad (2)$$

where $h_{pq}^{\text{LoS}}(t)$ and $h_{pq}^{\text{V-LoS}}(t)$ denote the small-scale channel coefficient for the (p, q) -th antenna pair of the LoS link and that of the V-LoS link through RIS, respectively. The $1/\Omega_{\text{LoS}}(t)$ and $1/\Omega_{\text{RIS}}(t)$ denote the large-scale path loss of the LoS link and that of V-LoS link through RIS, respectively, with $\Omega_{\text{LoS}}(t)$ and $\Omega_{\text{RIS}}(t)$ being the corresponding path power gains. In addition, $\tau^{\text{LoS}}(t) = \xi_{\text{TR}}(t)/c$ and $\tau^{\text{V-LoS}}(t) = (\xi_{\text{RIS}}^T + \xi_{\text{RIS}}^R(t))/c$ represent the path delay of the LoS link and that of V-LoS link through RIS, respectively, with $c = 3.0 \times 10^8$ m/s.

For the LoS link, the $h_{pq}^{\text{LoS}}(t)$ is expressed as

$$h_{pq}^{\text{LoS}}(t) = e^{-j\frac{2\pi}{\lambda}\xi_{\text{TR}}(t)} \times e^{j\frac{2\pi}{\lambda}v_R t \cos(\alpha_R^{\text{LoS}}(t) - \gamma_R)} \cos \beta_R^{\text{LoS}}(t) \times e^{j\frac{2\pi}{\lambda}\langle \mathbf{e}_T^{\text{LoS}}(t), \mathbf{d}_p^T \rangle} \times e^{j\frac{2\pi}{\lambda}\langle \mathbf{e}_R^{\text{LoS}}(t), \mathbf{d}_q^R \rangle}, \quad (3)$$

where λ is wavelength, $\xi_{\text{TR}}(t) = \{\xi_R + v_R t \cos \gamma_R\}^2 + H_0^2 + v_R^2 t^2 \sin^2 \gamma_R\}^{1/2}$, $\mathbf{d}_p^T = \frac{M_T-2q+1}{2} \delta_T [\cos \phi_T \cos \psi_T, \cos \phi_T \sin \psi_T, \sin \phi_T]^T$, and $\mathbf{d}_q^R = \frac{M_R-2q+1}{2} \delta_R [\cos \phi_R \cos \psi_R, \cos \phi_R \sin \psi_R, \sin \phi_R]^T$, respectively. Moreover, the unit direction vector at the BS, that is, $\mathbf{e}_T^{\text{LoS}}(t)$, and that at the MR, i.e., $\mathbf{e}_R^{\text{LoS}}(t)$, can be expressed as

$$\mathbf{e}_{T/R}^{\text{LoS}}(t) = \begin{bmatrix} \cos \beta_{T/R}^{\text{LoS}}(t) \cos \alpha_{T/R}^{\text{LoS}}(t) \\ \cos \beta_{T/R}^{\text{LoS}}(t) \sin \alpha_{T/R}^{\text{LoS}}(t) \\ \sin \beta_{T/R}^{\text{LoS}}(t) \end{bmatrix}, \quad (4)$$

in which, the time-varying angles are expressed as

$$\beta_R^{\text{LoS}}(t) = -\beta_T^{\text{LoS}}(t), \quad (5)$$

$$\beta_T^{\text{LoS}}(t) = \arcsin \{-H_0/\xi_{\text{TR}}(t)\}, \quad (6)$$

$$\alpha_R^{\text{LoS}}(t) = \begin{cases} \alpha_T^{\text{LoS}}(t) - \pi, & \text{if } \alpha_T^{\text{LoS}}(t) > 0 \\ \alpha_T^{\text{LoS}}(t) + \pi, & \text{if } \alpha_T^{\text{LoS}}(t) \leq 0, \end{cases} \quad (7)$$

$$\alpha_T^{\text{LoS}}(t) = \arcsin \frac{v_R t \sin \gamma_R}{\sqrt{(\xi_R + v_R t \cos \gamma_R)^2 + v_R^2 t^2 \sin^2 \gamma_R}}. \quad (8)$$

Moreover, the path power gain $\Omega_{\text{LoS}}(t)$ is expressed as

$$\Omega_{\text{LoS}}(t) = \frac{\lambda^2}{(4\pi)^2 \xi_{\text{TR}}^2(t)}. \quad (9)$$

For the V-LoS link through RIS, the small-scale fading channel coefficient $h_{pq}^{\text{V-LoS}}(t)$ can be expressed as [11]

$$h_{pq}^{\text{V-LoS}}(t) = \sqrt{\frac{1}{\Upsilon(t)}} \sum_{m=1}^M \sum_{n=1}^N \chi_{mn}(t) e^{j\varphi_{mn}(t)} \\ \times e^{-j\frac{2\pi}{\lambda}(\xi_{mn}^T + \xi_{mn}^R(t))} \times e^{j\frac{2\pi}{\lambda}v_R t \cos(\alpha_{\text{RIS}}^R(t) - \gamma_R) \cos \beta_{\text{RIS}}^R(t)} \\ \times e^{j\frac{2\pi}{\lambda}\langle e_T^{\text{RIS}}, d_p^T \rangle} \times e^{j\frac{2\pi}{\lambda}\langle e_R^{\text{RIS}}(t), d_q^R \rangle}, \quad (10)$$

in which the normalized factor $\Upsilon(t)$ is expressed as

$$\Upsilon(t) = \mathbb{E} \left\{ \left| \sum_{m=1}^M \sum_{n=1}^N \Gamma_{mn}(t) e^{-j\frac{2\pi}{\lambda}(\xi_{mn}^T + \xi_{mn}^R(t))} \right|^2 \right\}. \quad (11)$$

where $\Gamma_{mn}(t) = \chi_{mn}(t) e^{j\varphi_{mn}(t)}$. The unit direction vectors e_T^{RIS} and $e_R^{\text{RIS}}(t)$ in (10) can be obtained from (4) by replacing $\{\beta_T^{\text{LoS}}(t), \alpha_T^{\text{LoS}}(t)\}$ and $\{\beta_R^{\text{LoS}}(t), \alpha_R^{\text{LoS}}(t)\}$ with $\{\beta_{\text{RIS}}^T, \alpha_{\text{RIS}}^T\}$ and $\{\beta_{\text{RIS}}^R(t), \alpha_{\text{RIS}}^R(t)\}$, respectively. Moreover, the expressions of $\{\beta_{\text{RIS}}^R(t), \beta_{\text{RIS}}^T, \alpha_{\text{RIS}}^T, \alpha_{\text{RIS}}^R(t)\}$ can be referred to eqs. (9)-(12) in [11] by imposing $v_T = 0$ and they are omitted here for brevity.

Finally, the ξ_{mn}^T and $\xi_{mn}^R(t)$ in (11) can be expressed as

$$\xi_{mn}^T \approx \xi_{\text{RIS}}^T - 0.5(2m - M - 1)d_c \sin \beta_i \cos \alpha_i \\ - 0.5(2n - N - 1)d_r \sin \beta_i \sin \alpha_i, \quad (12)$$

$$\xi_{mn}^R(t) \approx \xi_{\text{RIS}}^R(t) - 0.5(2m - M - 1)d_c \sin \beta_o(t) \cos \alpha_o(t) \\ - 0.5(2n - N - 1)d_r \sin \beta_o(t) \sin \alpha_o(t), \quad (13)$$

where the expressions of $\{\alpha_i, \beta_i, \alpha_o(t), \beta_o(t)\}$ can be referred to Appendix B in [11] by imposing $v_T = 0$ and are omitted here for brevity. Moreover, $\xi_{\text{RIS}}^T = \{x_I^2 + y_I^2 + (z_I - H_0)^2\}^{\frac{1}{2}}$ and $\xi_{\text{RIS}}^R(t) = \{(x_I - \xi_R - v_R t \cos \gamma_R)^2 + (y_I - v_R t \sin \gamma_R)^2 + z_I^2\}^{\frac{1}{2}}$.

Furthermore, the large-scale path power gain of the V-LoS link through RIS can be expressed as [11]

$$\Omega_{\text{RIS}}(t) = \frac{\lambda^2 d_c d_r \cos \beta_i}{(4\pi)^3 \xi_{\text{RIS}}^T \xi_{\text{RIS}}^R(t)} \times \Upsilon(t). \quad (14)$$

III. PROPOSED TRANSMISSION MODE SWITCH SCHEME

We assume that exact and instantaneous channel state information (CSI) is available, and assume that the RIS reflection phase can be optimally configured to offset the phase difference of different units and that of different paths. Without considering time evolution, the achievable rate of the proposed model can be expressed as [10]

$$R = \log_2 \left(1 + \frac{M_T M_R P_T (\Omega_{\text{RIS}}^{\text{opt}} + \Omega_{\text{LoS}})}{\sigma^2} \right), \quad (15)$$

where $\Omega_{\text{RIS}}^{\text{opt}}$ is derived from (14) by imposing $\Upsilon(t) = M^2 N^2$. Formula (15) shows that the achievable rate is maximized when the BS utilizes V-LoS and LoS paths simultaneously for transmission thanks to their constructive combination. This kind of transmission mode requires complicated transmit power allocation. In addition, owing to the motion of the MR, the path power gains ($\Omega_{\text{RIS}}^{\text{opt}}$ and Ω_{LoS}) will vary and their difference may be very large, resulting in negligible capacity gain of utilizing two paths relative to utilizing one path for transmission. To this end, we propose a transmission mode switch scheme by exploiting the mapping relationship between BS transmission mode and MR location established in the offline

TABLE II
BS TRANSMISSION MODE DEFINITIONS

Setting	Description
RIS mode	BS performs transmit beamforming towards RIS and then RIS reflects the incident waves towards MR via passive beamforming
LoS mode	BS performs transmit beamforming towards MR directly via the LoS path between BS and MR
R&L mode	BS performs transmit beamforming towards MR via V-LoS and LoS paths simultaneously with power allocation

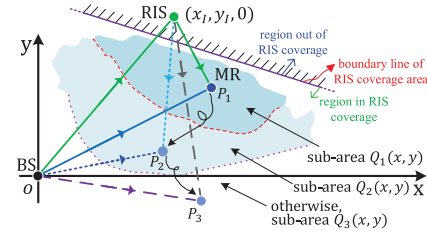


Fig. 3. Illustration of the area devision (top view), where P_1 , P_2 , and P_3 denote MR location in different sub-areas.

stage. Specifically, we define three BS transmission modes, they are, **RIS mode**, **R&L mode**, and **LoS mode**, as summarized in Table II. As the reflection-type RIS is adopted, only half of the ground surface area is within the RIS coverage. The entire RIS coverage area is further divided into three sub-areas, they are, $Q_1(x, y)$, $Q_2(x, y)$, and $Q_3(x, y)$, as depicted in Fig. 3. When the MR moves into different sub-areas in the online stage, the BS adopts different transmission modes utilizing different transmit beamforming vectors. For example, when the MR follows the trajectory of $P_1 \rightarrow P_2 \rightarrow P_3$, the corresponding BS transmission mode will be **RIS mode**→**R&L mode**→**LoS mode**, respectively. When LoS path disappears, on the other hand, **RIS mode** is applied.

For a MR with arbitrary location $(x, y, z = 0)$, we define the path power gain ratio between V-LoS and LoS links as

$$\eta = \frac{\Omega_{\text{RIS}}^{\text{opt}}}{\Omega_{\text{LoS}}} = A_{\text{RIS}} \times \frac{x^2 + y^2 + H_0^2}{(x - x_I)^2 + (y - y_I)^2 + z_I^2}, \quad (16)$$

where $A_{\text{RIS}} = \frac{d_c d_r M^2 N^2 \cos \beta_i}{4\pi \xi_{\text{RIS}}^T}$. It indicates that the power gain ratio η is dependent on MR location, resulting in MR location dependent achievable rate. In the following, we will figure out the mapping relationship between BS transmission mode and MR location sub-area based on this property.

Fig. 4 summarizes the proposed BS transmission mode switch scheme. We start by deriving the RIS coverage area. Note that the plane equation of the RIS surface can be expressed as

$$\begin{aligned} \sin \theta_I \cos \epsilon_I (x - x_I) - \cos \theta_I \cos \epsilon_I (y - y_I) \\ - \sin \epsilon_I (z - z_I) = 0. \end{aligned} \quad (17)$$

By imposing $z = 0$ in (17), the RIS coverage area, denoted by $Q_0(x, y)$, can be expressed as

$$Q_0(x, y) = \begin{cases} \sin \theta_I x - \cos \theta_I y + g_0 > 0, & \text{if } y_I > 0 \\ \sin \theta_I x - \cos \theta_I y + g_0 < 0, & \text{if } y_I < 0, \end{cases} \quad (18)$$

where $g_0 = -\sin \theta_I x_I + \cos \theta_I y_I + \tan \epsilon_I z_I$.

i) **RIS mode**: When MR is in sub-area $Q_1(x, y)$, the path power gain of V-LoS link is much larger than that of LoS link, i.e., $\eta \geq \eta_2 \gg 1$, where η_2 is the upper threshold, causing $1/\eta + 1 \approx 1$. The achievable rate in (15) is approximated by

$$R \approx \log_2 (1 + M_T M_R P_T \Omega_{\text{RIS}}^{\text{opt}} / \sigma^2), \quad (19)$$

indicating that the capacity gain from LoS path is negligible. Therefore, the BS adopts the **RIS mode** for transmission, and the BS transmit beamforming vector can be expressed as

$$\mathbf{f}_{\text{BS}}^{\text{RIS}} = \frac{1}{\sqrt{M_T}} [e^{-j\frac{2\pi}{\lambda} \langle \mathbf{e}_T^{\text{RIS}}, \mathbf{d}_{p=1}^T \rangle}, \dots, e^{-j\frac{2\pi}{\lambda} \langle \mathbf{e}_T^{\text{RIS}}, \mathbf{d}_{M_T}^T \rangle}]^T. \quad (20)$$

Moreover, by employing $\eta \geq \eta_2$, (16) yields

$$A_{\text{RIS}} \times \frac{x^2 + y^2 + H_0^2}{(x - x_I)^2 + (y - y_I)^2 + z_I^2} \geq \eta_2, \quad (21)$$

which results in the area region of $Q'_1(x, y)$ in (22), as shown at the bottom of the page. Then, the MR location sub-area region for BS adopts **RIS mode** can be expressed as

$$Q_1(x, y) = Q_0(x, y) \cap Q'_1(x, y). \quad (23)$$

Note that when LoS path disappears, BS also adopts the **RIS mode**.

ii) **LoS mode**: When MR is in sub-area $Q_3(x, y)$, the path power gain of V-LoS link is much smaller than that of LoS link, i.e., $\eta \leq \eta_1 \ll 1$ with η_1 being the lower threshold, resulting in $1 + \eta \approx 1$. Thus, (15) can be approximated by

$$R \approx \log_2 (1 + M_T M_R P_T \Omega_{\text{LoS}} / \sigma^2), \quad (24)$$

implying that the capacity gain from V-LoS link becomes negligible. Then, the BS adopts the **LoS mode** for transmission, and the corresponding BS transmit beamforming vector, denoted by $\mathbf{f}_{\text{BS}}^{\text{LoS}}$, can be derived from (20) by replacing $\mathbf{e}_T^{\text{RIS}}$ with $\mathbf{e}_T^{\text{LoS}}$.

Similarly, by setting $\eta \leq \eta_1$ in (16), we have

$$A_{\text{RIS}} \times \frac{x^2 + y^2 + H_0^2}{(x - x_I)^2 + (y - y_I)^2 + z_I^2} \leq \eta_1, \quad (25)$$

which yields the area region of $Q'_3(x, y)$ in (26), as shown at the bottom of the page. Therefore, the MR location sub-area region for BS adopts **LoS mode** is expressed as

$$Q_3(x, y) = Q_0(x, y) \cap Q'_3(x, y). \quad (27)$$

iii) **R&L mode**: Otherwise, when MR is in sub-area $Q_2(x, y)$, i.e., $\eta_1 < \eta < \eta_2$, the capacity gains from both V-LoS and LoS links should be considered. In this case, the BS applies the **R&L mode** for transmission, and therefore the BS transmit beamforming vector can be expressed as

$$\mathbf{f}_{\text{BS}}^{\text{R&L}} = \sqrt{\frac{\Omega_{\text{RIS}}^{\text{opt}}}{\Omega_{\text{LoS}} + \Omega_{\text{RIS}}^{\text{opt}}}} \mathbf{f}_{\text{BS}}^{\text{RIS}} + \sqrt{\frac{\Omega_{\text{LoS}}}{\Omega_{\text{LoS}} + \Omega_{\text{RIS}}^{\text{opt}}}} \mathbf{f}_{\text{BS}}^{\text{LoS}}. \quad (28)$$

$$Q'_1(x, y) = \begin{cases} (x + \frac{\eta_2 x_I}{A_{\text{RIS}} - \eta_2})^2 + (y + \frac{\eta_2 y_I}{A_{\text{RIS}} - \eta_2})^2 \geq \frac{A_{\text{RIS}} \eta_2 (x_I^2 + y_I^2 + z_I^2) - \eta_2^2 z_I^2 - (A_{\text{RIS}} - \eta_2) A_{\text{RIS}} H_0^2}{(A_{\text{RIS}} - \eta_2)^2}, & \text{if } A_{\text{RIS}} > \eta_2 \\ 2x_I x + 2y_I y + H_0^2 - (x_I^2 + y_I^2 + z_I^2) \geq 0, & \text{if } A_{\text{RIS}} = \eta_2 \\ (x + \frac{\eta_2 x_I}{A_{\text{RIS}} - \eta_2})^2 + (y + \frac{\eta_2 y_I}{A_{\text{RIS}} - \eta_2})^2 \leq \frac{A_{\text{RIS}} \eta_2 (x_I^2 + y_I^2 + z_I^2) - \eta_2^2 z_I^2 - (A_{\text{RIS}} - \eta_2) A_{\text{RIS}} H_0^2}{(A_{\text{RIS}} - \eta_2)^2}, & \text{if } A_{\text{RIS}} < \eta_2 \end{cases} \quad (22)$$

$$Q'_3(x, y) = \begin{cases} (x + \frac{\eta_1 x_I}{A_{\text{RIS}} - \eta_1})^2 + (y + \frac{\eta_1 y_I}{A_{\text{RIS}} - \eta_1})^2 \leq \frac{A_{\text{RIS}} \eta_1 (x_I^2 + y_I^2 + z_I^2) - \eta_1^2 z_I^2 - (A_{\text{RIS}} - \eta_1) A_{\text{RIS}} H_0^2}{(A_{\text{RIS}} - \eta_1)^2}, & \text{if } A_{\text{RIS}} > \eta_1 \\ 2x_I x + 2y_I y + H_0^2 - (x_I^2 + y_I^2 + z_I^2) \leq 0, & \text{if } A_{\text{RIS}} = \eta_1 \\ (x + \frac{\eta_1 x_I}{A_{\text{RIS}} - \eta_1})^2 + (y + \frac{\eta_1 y_I}{A_{\text{RIS}} - \eta_1})^2 \geq \frac{A_{\text{RIS}} \eta_1 (x_I^2 + y_I^2 + z_I^2) - \eta_1^2 z_I^2 - (A_{\text{RIS}} - \eta_1) A_{\text{RIS}} H_0^2}{(A_{\text{RIS}} - \eta_1)^2}, & \text{if } A_{\text{RIS}} < \eta_1 \end{cases} \quad (26)$$

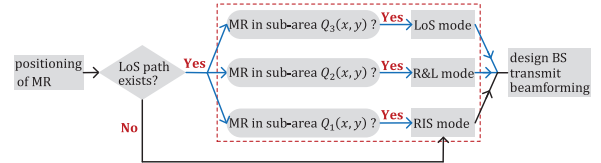


Fig. 4. Flowchart of the proposed switch scheme.

Furthermore, the MR location sub-area region for BS employing **R&L mode** for transmission can be expressed as

$$Q_2(x, y) = Q_0(x, y) \ominus (Q_1(x, y) \cup Q_3(x, y)). \quad (29)$$

IV. RESULTS AND DISCUSSIONS

The simulation parameters are based on the existing work [11] except that the transmitter is a static BS in this letter. Furthermore, we set $P_T = 10$ dBm, $\sigma^2 = -80$ dBm, $H_0 = 20$ m, $(x_I, y_I, z_I) = (40$ m, 40 m, 15 m), $M = N = 270$, $\theta_I = -\frac{\pi}{18}$, $\epsilon_I = 0$, $\eta_1 = 0.1$, and $\eta_2 = 10$, respectively.

We illustrate the mapping relationship between BS transmission mode and MR location in Fig. 5. With the basic parameter setting, Fig. 5(a) indicates that the RIS coverage area is divided into three sub-areas, they are, sub-areas $Q_1(x, y)$, $Q_2(x, y)$, and $Q_3(x, y)$, respectively. When the MR moves into different sub-areas, the BS directly switches its transmission mode by applying corresponding transmit beamforming vector based on the location information of MR. By varying the system setups, such as RIS unit number, RIS location, RIS orientation angles, and BS height, Figs. 5(b)-(f) show that the RIS coverage area as well as the sub-areas division will change, resulting in different mapping relationship between BS transmission mode and MR location. Fig. 5(f) indicates that under discrete phase shifts with two controlling bits, the location and size of sub-area will change, but the squared power gain of RIS as well as the basic mapping relationship between BS transmission mode and MR location still hold [12], [13].

Fig. 6 shows the time-varying achievable rate of the proposed switch scheme, where the MR moves from $P_3(0, -5$ m) in $Q_3(x, y)$ to $P_1(43$ m, 37 m) in $Q_1(x, y)$. Accordingly, we set $v_R = 6$ m/s and $\gamma_R = \arctan\{42/43\}$. Under this moving trajectory, the MR will firstly experience sub-area $Q_3(x, y)$ adopting **LoS mode**, then sub-area $Q_2(x, y)$ adopting **R&L mode**, and finally sub-area $Q_1(x, y)$ adopting **RIS mode**. The results show that the system with RIS outperforms the system without RIS, which highlights the capability of RIS in capacity improvement [6]. By exploiting the extra reappearing LoS path, the achievable rate of the proposed switch scheme outperforms that of RIS-assisted mmWave systems with blocking LoS path in [3]. With the proposed switch scheme, the RIS auxiliary system will approach optimal performance with lower online signal processing complexity.

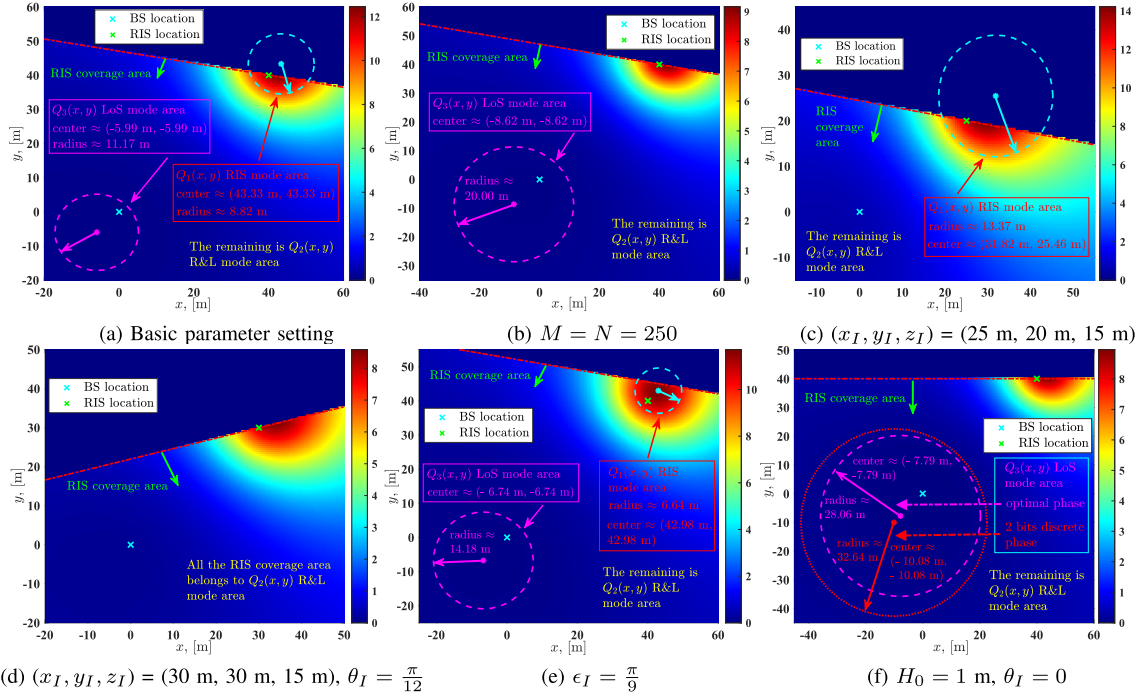


Fig. 5. Mapping relationship between BS transmission mode and MR location under different system setups.

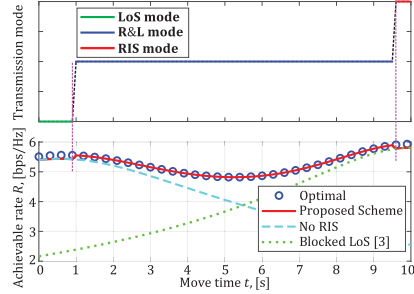


Fig. 6. Achievable rate of the proposed switch scheme, parameter setting is the same as in Fig. 5(a).

V. CONCLUSION

In this letter, we have considered a RIS auxiliary mmWave mobile communication system with alternately disappearing and reappearing LoS path due to the motion of the MR. An online BS transmission mode switch scheme is developed for transmit beamforming vector design based on the time-varying location of the MR, by exploiting the mapping relationship between BS transmission mode and MR location established in the offline stage. The results show that the proposed scheme realizes near-optimal performance, and the system setup, such as RIS location, units number, and orientation angles, etc., will affect the mapping relationship, which provides guidelines for future RIS auxiliary mmWave mobile systems design. As future work, we can mathematically prove that RIS with discrete phase shifts also achieves squared power gain.

REFERENCES

- [1] T. S. Rappaport et al., "Millimeter wave mobile communications for 5G cellular: It will work!" *IEEE Access*, vol. 1, pp. 335–349, 2013.
- [2] E. Basar, M. Di Renzo, J. De Rosny, M. Debbah, M.-S. Alouini, and R. Zhang, "Wireless communications through reconfigurable intelligent surfaces," *IEEE Access*, vol. 7, pp. 116753–116773, 2019.
- [3] N. S. Perović, M. Di Renzo, and M. F. Flanagan, "Channel capacity optimization using reconfigurable intelligent surfaces in indoor mmWave environments," in *Proc. IEEE ICC*, Dublin, Ireland, Jun. 2020, pp. 1–7.
- [4] H. Du, J. Zhang, J. Cheng, and B. Ai, "Millimeter wave communications with reconfigurable intelligent surfaces: Performance analysis and optimization," *IEEE Trans. Commun.*, vol. 69, no. 4, pp. 2752–2768, Apr. 2021.
- [5] A. Chen, Y. Chen, and Z. Wang, "Reconfigurable intelligent surface deployment for blind zone improvement in mmWave wireless networks," *IEEE Commun. Lett.*, vol. 26, no. 6, pp. 1423–1427, Jun. 2022.
- [6] Q. Wu and R. Zhang, "Intelligent reflecting surface enhanced wireless network via joint active and passive beamforming," *IEEE Trans. Wireless Commun.*, vol. 18, no. 11, pp. 5394–5409, Nov. 2019.
- [7] B. Xiong et al., "A statistical MIMO channel model for reconfigurable intelligent surface assisted wireless communications," *IEEE Trans. Commun.*, vol. 70, no. 2, pp. 1360–1375, Feb. 2022.
- [8] A. Goldsmith, *Wireless Communications*, Cambridge, U.K.: Cambridge Press, 2005.
- [9] O. El Ayach, S. Rajagopal, S. Abu-Surra, Z. Pi, and R. W. Heath Jr., "Spatially sparse precoding in millimeter wave MIMO systems," *IEEE Trans. Wireless Commun.*, vol. 13, no. 3, pp. 1499–1513, Mar. 2014.
- [10] C. Huang, A. Zappone, G. C. Alexandropoulos, M. Debbah, and C. Yuen, "Reconfigurable intelligent surfaces for energy efficiency in wireless communication," *IEEE Trans. Wireless Commun.*, vol. 18, no. 8, pp. 4157–4170, Aug. 2019.
- [11] B. Xiong, Z. Zhang, H. Jiang, J. Zhang, L. Wu, and J. Dang, "A 3D non-stationary MIMO channel model for reconfigurable intelligent surface auxiliary UAV-to-ground mmWave communications," *IEEE Trans. Wireless Commun.*, vol. 21, no. 7, pp. 5658–5672, Jul. 2022.
- [12] H. Zhang, B. Di, L. Song, and Z. Han, "Reconfigurable intelligent surfaces assisted communications with limited phase shifts: How many phase shifts are enough?" *IEEE Trans. Veh. Technol.*, vol. 69, no. 4, pp. 4498–4502, Apr. 2020.
- [13] Y. Shuang et al., "One-bit quantization is good for programmable coding metasurfaces," *Sci. China Inf. Sci.*, vol. 65, no. 1, pp. 1–15, Jul. 2022.